

Iron K Lines from Gamma Ray Bursts

T. R. Kallman¹, P. Mészáros² & M.J. Rees³

¹NASA Goddard Space Flight Center, LHEA, Code 665, Greenbelt, MD 20771

²Dpt. Astron. & Astrophysics, Pennsylvania State University, University Park, PA 16803

³Inst. of Astronomy, Cambridge University, Madingley Road, Cambridge CB3 0HA, U.K.

Oct. 23, 2001

ABSTRACT

We present models for reprocessing of an intense flux of X-rays and gamma rays expected in the vicinity of gamma ray burst sources. We consider the transfer and reprocessing of the energetic photons into observable features in the X-ray band, notably the K lines of iron. Our models are based on the assumption that the gas is sufficiently dense to allow the microphysical processes to be in a steady state, thus allowing efficient line emission with modest reprocessing mass and elemental abundances ranging from solar to moderately enriched. We show that the reprocessing is enhanced by down-Comptonization of photons whose energy would otherwise be too high to absorb on iron, and that pair production can have an effect on enhancing the line production. While “distant” reprocessors such as supernova or wind remnants require Fe abundances much larger than solar to reproduce the observed line luminosities, we show that “nearby” reprocessor models, involving e.g. outer stellar envelopes, can do so with solar or only modestly enriched abundances.

1. Introduction

The discovery of iron K line emission from the afterglows of cosmic gamma-ray burst sources (GRBs) provides a potentially important diagnostic of redshift as well as conditions in the burst environment. The measured line intensities, together with distance estimates, constrain the total number of iron decays needed to produce the line. A plausible assumption is that the line is formed by reprocessing of continuum photons from the burst itself or its later outflow by gas which is separate from the continuum-producing region, so that the temperature and ionization are determined by those continuum photons. If so, the time delay between the burst and the line detection provides constraints on the timescales

for recombination, level decay and light travel time between the source of continuum source and reprocessor. However, accurate calculations of the reprocessing of the burst continuum spectrum into lines is potentially complicated owing to the possible effects of radiative transfer, time dependent atomic processes affecting line formation and the gas temperature.

The statistical quality of the observations so far are not sufficient to establish a unique model which can fit the available data. A key point is that the extremely large photon fluences near a GRB are likely to be sufficient to completely ionize the nearby gas in a time which is short compared with the duration of the burst. An important criterion for evaluating any model is the reprocessing efficiency, i.e. the ratio of the iron line fluence to the continuum fluence from the burst. Under a wide range of assumptions regarding the burst continuum flux and the reprocessor density the ionization parameter $\xi = L_{inc}/nr^2$ must exceed $\sim 10^3$ (see §2.2), where r is the distance to the source and n is the particle density. The other important observational constraint is the time at which the line emission becomes most prominent, typically several hours to a day for Fe emission features (e.g. Piro, *et al.*, 2000). This places severe constraints on the reprocessing gas and has, so far, divided the models into distinct classes distinguished by assumptions regarding the density, thickness and composition of the reprocessing material.

In the “distant reprocessor” scenario it is assumed that the gas illuminated by the burst and afterglow continuum is far enough for the time delay to be due to light travel time differences. In order to achieve the required high ionization parameter, this involves reprocessing of the prompt burst emission, with luminosities of order 10^{50} erg/sec. The timescale for line emission per ion is not very short compared to the burst duration, so the reprocessing efficiencies are low if the iron abundance is solar, requiring therefore material which is highly enriched in iron in order to account for Fe line observations. Such conditions are expected to occur in models with a distant shell or ring (e.g. Weth, *et al.*, 2000, Böttcher, 2000, Böttcher & Fryer, 2001), possibly associated with supernova events (e.g. the supranova model of Vietri *et al.*, 2001).

On the other hand, “nearby reprocessor” scenarios are capable of much greater reprocessing efficiencies, if the distances and gas densities are assumed to be comparable to those in extended stellar envelopes, or in dense, thick media similar to those in the reprocessors near accreting X-ray sources. In this scenario, iron enrichment is not required, and the timescales are sufficiently short that many Fe line photons are produced per Fe ion during the afterglow phase of the burst. Incident luminosities of order 10^{47} erg/s are required at timescales comparable to a day, and radiative transfer effects are important. Such conditions are expected, e.g., in the decaying jet model of Rees and Mészáros (2000), and in the jet plus bubble model of Mészáros and Rees (2001), which differ in the origin of

the non-thermal component which is reprocessed by gas at distances comparable to outer stellar envelope.

In this paper we present models which analyze these two generic families of models, with an added emphasis on the case of nearby reprocessors. In the following sections we present in turn the physics of line formation, our modelling technique, results, and a discussion of some implications.

2. Background

2.1. Observations

There are so far only a handful of observations of afterglows bright enough to allow unambiguous iron line detections (Piro et al., 1999, 2000; Yoshida et al., 1999). Owing to the limited number of photons, and to uncertainties about the source redshift and the time evolution of the line, the line flux is the best constrained observable quantity. Comparison with models requires conversion to luminosity, which is affected by the distance estimate. As an example, we focus on the observation of GRB991216 by Piro et al. (2000) and distance estimate given those authors giving $z=1.00 \pm 0.02$ and $D=4.7$ Gpc for $H_0 = 75$ km s $^{-1}$ and $q_0=0.5$. The maximum line luminosity was therefore $L_{line} \simeq 10^{53}$ photons s $^{-1}$ $\simeq 10^{45}$ erg s $^{-1}$, and a line fluence $\sim 10^{49}$ erg. As discussed by Piro et al. (2000), Lazzatti et al. (1999), Vietri et al. (2000) and others the total mass of iron required to produce this is $\sim 50M_\odot/n_{decays}$, where n_{decays} is the total number of decays per iron nucleus. This clearly demonstrates the tradeoff between n_{decays} and the implied emitting mass of iron. If $n_{decays} \gg 1$, then a moderate mass of iron is needed (e.g. Weth et al., 2000). Piro et al. (2000) also report a possible detection of a feature attributed to the recombination continuum (RRC) of hydrogen-line iron, Fe XXVI. This suggests that both features are emitted by recombination in highly ionized iron.

2.2. Ionization Equilibrium

If the line is emitted by reprocessing of burst continuum photons then the value n_{decays} cannot exceed the number of continuum photons absorbed per iron ion during the burst. This limit is achieved when both the recombination and photoionization timescales per ion are much less the duration of the burst. The recombination timescale from fully stripped into hydrogenic iron (case A) is approximately $t_{rec} \simeq 7n_{11}^{-1}T_8^{0.74}$ sec where n_{11} is the electron number density in units of 10^{11} cm $^{-3}$, and T_8 is the electron temperature in units of 10^8 K.

The photoionization timescale is $t_{PI} \simeq 2 \times 10^{-7} L_{47}^{-1} R_{13}^2$ s, where L_{47} is the continuum luminosity in units of 10^{47} erg s $^{-1}$ and R_{13} is the distance from the source to the reprocessor in units of 10^{13} cm, and we have assumed a power law ionizing spectrum between 1 and 1000 Ry with energy index 0.9. The preceding expression can be rewritten in terms of the ionization parameter $\xi = L/nR^2$ as $t_{PI} \simeq 2 \times 10^3 \xi^{-1} n_{11}^{-1}$ s. This demonstrates that for parameter choices $10^{11} \text{ cm}^{-3} \lesssim n \lesssim 10^{17} \text{ cm}^{-3}$ and $\xi \geq 10^3$ erg cm s $^{-1}$ the recombination timescale is greater than the photoionization timescale, but that both are short compared with the burst duration ($t_{burst} \sim 10 - 100$ s) or the delay between the burst and afterglow, delayed jet or bubble emergence ($t_{delay} \sim 10^5$ s). Therefore the gas can be regarded as being locally in ionization equilibrium: the level of ionization will adjust itself such that the ratio of ionized (fully stripped) to non-ionized (i.e. hydrogenic, helium-like, etc.) iron will be equal to t_{rec}/t_{PI} , and the value of this ratio is approximately $3 \times 10^{-3} T_8^{0.74} \xi$. This demonstrates that the gas will be highly ionized in equilibrium for ionization parameters $\xi \geq 10^3$ which, as we will show, are most plausible for GRB reprocessors.

2.3. Assumptions

In the remainder of this paper we focus on gas densities in this range $10^{11} \text{ cm}^{-3} \lesssim n \lesssim 10^{17} \text{ cm}^{-3}$. Such densities are comparable to those expected in massive progenitor models of GRB, e.g. in blobby “distant” shells (Weth et al 2000, Piro et al 2000), or “nearby” envelope remnants compressed by relativistic jets or emerging bubbles (Mészáros and Rees, 2001). In addition, we assume that the temperature, ionization, and excitation conditions in the reprocessing gas are determined solely by reprocessing of continuum photons from the burst or its afterglow components. This is equivalent to the assumption that the reprocessing gas is physically separate from the gas responsible for the burst continuum photons. In the “distant reprocessor” models ($R \geq 10^{15}$ cm) this naturally fits in with the observed $\sim 10^5$ s time lag between the burst and line detections, while in the “nearby reprocessor” models ($R \sim 10^{13}$ cm) this is related to the long-life of a jet or the late release of bubble ($\sim 10^5$ s).

We also assume that dynamical effects of the burst on the reprocessor are unimportant. Support for this comes from the fact that the sound crossing time for the most compact reprocessor we consider is ≥ 100 s, while the microphysical timescales are much shorter.

An added complication in comparing models with the data is the origin of the *observed* continuum in the vicinity of the line. Inherent in our models is the assumption that the line photons are emitted nearly isotropically; some anisotropy results from radiative transfer effects as the line photons escape the reprocessor, which we assume is a geometrically thin

and optically thick plane-parallel slab or thin shell (although we will also discuss alternatives to this in the next section). The continuum may be affected by relativistic beaming, and the continuum observed in the vicinity of the line may differ from the continuum at the same energy which is incident on the reprocessor. On the other hand, the detectability of the line depends on the equivalent width measured with respect to these continuum photons. In what follows we present model results and discussion using the quantity which is most closely related to the physics of the reprocessor: line luminosity. We also discuss estimates for the observed line equivalent width based on simple assumptions regarding the continuum radiation field and the reprocessor geometry.

2.4. Line Emission

Iron line emission in photoionized gas occurs primarily by recombination and inner shell fluorescence. The efficiency of fluorescence can be much greater than for recombination, but the ionization conditions required are less likely to be applicable to GRB reprocessors.

The efficiency of line emission by recombination is given by the product of the effective Fe XXVI La recombination rate coefficient and the emission measure ionized by the burst continuum. This quantity can be approximated as

$$L_{rec}/L_{inc} \simeq 4\pi N\alpha\varepsilon_{line}y_{Fe}x_{FeXXVII}/\xi \quad (1)$$

where L_{rec} is the line luminosity, L_{inc} is the incident ionizing continuum luminosity, N is the radial column density of the shell, $\alpha \simeq 3.4 \times 10^{-13} \text{ cm}^3\text{s}^{-1}$ is the effective recombination rate coefficient for production of the line, ε_{line} is the line energy, $x_{FeXXVII}$ is the ionization fraction of fully stripped iron, y_{Fe} is the iron abundance, and $\xi = L/nR^2$ is the ionization parameter (eg. Tarter Tucker and Salpeter, 1969). This quantity is the ratio of the line luminosity radiated by an optically thin spherical shell to the luminosity of the central exciting source, and it enters the equation because of the fact that the recombination emission rate is proportional to gas density. Inserting plausible numerical values gives

$$L_{rec}/L_{inc} \sim 1.4N_{24}y_{\odot}x_{FeXXVII}/\xi \quad (2)$$

where N_{24} is the column in units of 10^{24} cm^{-2} . The fractional abundance of highly ionized iron is negligible for ionization parameters $\xi \leq 10^3 \text{ erg cm sec}^{-1}$, so the maximum fractional recombination luminosity attainable is $\sim 10^{-3}$.

Inner shell fluorescence can occur if iron is not highly ionized, i.e. if the typical ion has 3 or more bound electrons. The luminosity is

$$L_{fl}/L_{inc} \simeq \omega_{fl} N \sigma_{PI} f_\varepsilon \frac{\Delta\varepsilon}{\varepsilon} \varepsilon_{line} y_{Fe} x_{\leq FeXXIV} \quad (3)$$

where ω_{fl} is the fluorescence yield (0.34 for neutral iron), σ_{PI} is the photoionization cross section at threshold, f_ε is the normalized spectral function at the K threshold energy (see Kallman and McCray 1980 for a definition), $\Delta\varepsilon/\varepsilon$ is a number of order unity which describes the fractional energy bandwidth contributing to the photoionization rate integral (for a power law with energy index α one has $\Delta\varepsilon/\varepsilon = 1/(3 + \alpha)$), and $x_{\leq FeXXIV}$ is the ionization fraction of all iron ions with 3 or more electrons. The rate for fluorescent line emission is proportional to the ionizing flux, so the efficiency is independent of ξ . Inserting plausible numbers gives

$$L_{fl}/L_{inc} \sim 0.005 N_{24} y_\odot x_{\leq FeXXIV} \quad (4)$$

for a single power law spectrum with an energy index of 0.9.

Another convenient measurement of line strength is the equivalent width measured with respect to the continuum incident on the reprocessor, given by

$$EW = (L_{line}/(L_{inc} f_\varepsilon)) \simeq (L_{line}/L_{inc}) \varepsilon_{line} \kappa \quad (5)$$

where κ is a numerical factor depending on the shape of the incident continuum, $\kappa \simeq 20$ for our choice of power law with energy index 0.9. This shows that fluorescence lines can have equivalent widths ~ 1 KeV, or fractional luminosities $\sim 10^{-3}$, but require low ionization parameter $\xi \leq 10^3$ erg cm s $^{-1}$.

For burst luminosities in the range $10^{47} - 10^{52}$ erg s $^{-1}$ and distances $\leq 10^{15}$ cm from the source, gas densities $\geq 10^{15} \xi_3^{-1} L_{48} R_{15}^{-2}$ are implied if $\xi \geq 10^3$. This is at the limit of what we consider in the models which follow. So, although fluorescence is included in all our models, it turns out to be generally less important than recombination, and the model equivalent widths (defined as in equation (5)) are less than the maximum attainable.

3. Computational technique

More accurate treatments of gamma-ray reprocessing and iron line emission require calculations of the ionization balance and electron kinetic temperature in the gas, along with the emission measure of gas which can emit lines. Calculation of ionization balance and temperature is straightforward given the local mean intensity of ionizing photons; calculating the transfer of these photons is complicated owing to scattering and attenuation by Compton scattering and photoelectric absorption. Compton scattering can redistribute photons from high energies ($\gtrsim 1$ MeV) to energies where photoelectric absorption is important, and absorption depends on the local ionization balance. In addition, high energy photons can produce e^+e^- pairs by collision with lower energy reprocessed photons, and these pairs can affect the ionization balance of iron by contributing to recombination, as well as contributing to Compton scattering of continuum photons. An accurate treatment of all these process requires a numerical solution.

The problem of reprocessing of gamma rays and hard X-rays and iron line formation does not lend itself easily to most of the numerical techniques developed for treating either photoionized reprocessing or Comptonization. This is because Compton scattering is likely to be important if the column density of the reprocessor is large (eg. $\geq 10^{24}$ cm $^{-2}$) and because the scattering must be treated relativistically in order to accurately treat the gamma rays with energies $\gtrsim 1$ MeV. Models developed for iron line formation in AGN accretion disks (see, for example, Nayakshin et al., 2000 and Ballantyne et al. 2000) which utilize Fokker-Planck or convolution methods for Comptonization are not highly accurate if these gamma rays are important. At the same time, the reprocessing gas temperature must be $\sim 10^8$ K or less, owing to limits on broadening of the observed lines, so that models developed for relativistic plasmas (e.g. Coppi and Blandford 1990) are also not directly applicable.

The reprocessing of gamma rays can affect the iron K line production in two ways. First, down-Comptonization in a gas with mean electron energy which is small compared with the gamma ray energy will soften the spectrum in the interior of the reprocessor. This can enhance the production of line photons owing to the increase in the cross section for iron photoionization at low energies. In addition, incident gamma rays at energies greater than ~ 1 MeV can produce pairs by $\gamma - \gamma$ collisions with reflected photons, if the center of mass energy is greater than the threshold for this process. This can enhance the rate of recombination onto iron, and can also change the mean free path for Compton scattering.

The models presented here make use of the Monte-Carlo technique for treating the transfer of continuum photons. This has the advantage that it allows for exact treatment of the relativistic rates and cross sections for Compton scattering and photon destruction, and

that pair production can be incorporated in a straightforward way. We use the Monte-Carlo code is described in Hua (1997), with modifications to allow for photoabsorption and pair production.

In order to calculate line formation and photoelectric absorption it is necessary to combine the photon flux derived from the Monte-Carlo calculation with a calculation of the heating, ionization, and excitation of the gas. To do so we use a photoionization equilibrium model (xstar; Kallman and Bautista 2000), using the ionizing flux from the Monte-Carlo calculation at each point in the cloud. This calculation is iteratively repeated 3-5 times in order to self-consistently account for photoelectric absorption and Compton scattering. Transfer of the line photons and thermal continuum photons escaping the cloud is calculated using the xstar escape probability formalism to calculate the local escaping flux, and then Comptonization of the line is calculated using an additional Monte-Carlo step.

Input parameters are: ionization parameter ξ , the continuum spectral shape which we take to be single power law with energy index -0.9 from 0.1 eV to 20 MeV, gas density and elemental composition. The ionization parameter is defined in terms of the incident energy flux of photons and the gas density, $\xi = 4\pi F/n$, where $F = \int_{13.6eV}^{13.6keV} F_\varepsilon d\varepsilon$. The total incident photon number flux is $F_{inc}^{(n)} = \int_0^\infty F_\varepsilon / \varepsilon d\varepsilon$. The chemical composition should be model- and assumption-dependent, hence a conventional choice (which also fits in well with nearby reprocessor scenarios) is used, [H:He:C:O:Ne:Si:S:Fe]=[12:11:8.65:8.87:8.14:7.57:7.28:7.50] (Morrison and McCammon 1981).

We perform the Monte Carlo transfer calculation for a total number of photons N_{tot} (100 photons per energy bin for each of 500 bins) to get the number distribution of photons vs. depth and energy $N(\varepsilon, z)$. At each scattering the cross sections for Compton scattering (fully relativistic in both photon and electron energy), photoelectric absorption, and pair production (described in more detail in the following section) are calculated. The fate of the photon is determined by calculating the path length for each process, also including escape, and taking the smallest. Then the number distribution of photons vs. depth and energy is converted to a local energy flux using $F_{local}(\varepsilon, z) = F_{inc}^{(n)} N(\varepsilon, z) / N_{tot}$. This then used to calculate the ionization balance and temperature throughout the slab using xstar. Compton heating and cooling is calculated fully relativistically using the results of Guilbert (1986). Both Monte-Carlo and photoionization steps are repeated a number of times (~ 4) to self-consistently calculate transfer, ionization, pair production/annihilation, etc.

4. Model results

The key issues we wish to address with these models are:

- 1) What is the penetration of the gamma rays and X-rays into the reprocessor, along with the down-Comptonization of gamma rays?
- 2) What is the albedo of the reprocessor to gamma rays, and the spectrum of the reflected gammas?
- 3) What is the efficiency of iron line emission, and does it scale with ξ as predicted by equations (2) and (4)?

To address these issues, we have run the models summarized in Table 1. These span a range of ionization parameter, and include models designed to test some of the assumptions described so far. The reprocessor distance range is $10^{13} - 10^{16}$ cm, the gas densities are $10^{11} - 10^{17}$ cm $^{-3}$, and the incident continuum luminosity range is $10^{46} - 10^{52}$ erg s $^{-1}$. The smaller distance is comparable to a massive stellar stellar envelope, while the densities range from those which might be encountered in clumpy blobs of a $\sim 1M_{\odot}$ shell at a light-day distance, up to typical atmospheric or clumpy ejecta densities at massive stellar envelope distances. The high values of incident luminosity L_{inc} are characteristic of the earlier epochs (minutes), while the lower ones are characteristic of later epochs (several hours to days). The ionizing spectrum, geometry, elemental abundances, and basic computational procedure were described in the previous section.

Table 1 presents the results of our model calculation: ionization parameter and iron line strength, both recombination alone (in the column labelled L_{Fe26}) and total (in the column labelled L_{Fe}). These line luminosities correspond to the total escaping line flux, without attempting to distinguish the un-Comptonized fraction. This issue is discussed in more detail later in this section.

In Figure 1 we plot these results as a function of ionization parameter for the nearby models. This shows the behavior predicted by equations (1) and (2), ie. that the line reprocessing efficiency decreases approximately inversely with increasing ionization parameter. For the “distant” models at $R=10^{16}$ cm we find that the $L_{line}/L_{inc} \propto \xi^{-0.75}$. Comparison of equation (2) with the line formation efficiencies in the table shows a difference of a factor $\sim 10 - 50$. This is due to the influence of Comptonization, which increases the flux of photons available to ionize iron and hence the line emitting volume. A further illustration is provided by the results of model 2nc, which was calculated with the same parameters as model 2, but using simple single stream exponential attenuation of the incident photons rather than using the Monte Carlo Comptonization calculation. The

model	$\log(n_p)$	$\log(r_{in})$	$\log(L_{in})$	$\log(\xi)$	$\log(L_{Fe26})$	$\log(L_{Fe})$	$\log(L_{Fe}^{(ns)})$	$\log(L_{Fe}^{(ns70)})$	note
1	17	13	46	3.	44.11	44.28	42.59	42.86	
2	17	13	47	4.	44.37	44.45	42.27	43.67	
2np	17	13	47	4.	44.37	44.57	42.46		1
2nc	17	13	47	4.	43.15	43.40	41.73		2
3	17	13	48	5.	44.77	44.99	42.34	43.47	
4	17	13	50	7.	45.51	45.64	42.25	44.07	
5	17	13	52	9.	45.69	45.79	42.11	43.97	
5np	17	13	52	9.	45.71	45.81	42.133		1
-	-	-	-	-	-	-	-	-	-
6	11	16	47	4.	44.29	44.55	42.40	43.72	
6ni	11	16	47	4.		44.88*			3
7	11	16	52	9.	45.91	46.04	42.28	44.05	
7np	11	16	52	9.	45.91	46.04	42.27		1

Table 1: Parameters and results for the “nearby” (models 1-5) and for the “distant” (models 6, 7) reprocessor scenarios. In the nearby reprocessor models (1-5) time delay effects are unimportant, and the observed line luminosities are those given in the L_{Fe26} and L_{Fe} columns (which refer to H-like and total Fe), for the incident continuum luminosities given in the L_{in} column (which gives the initial value of the 0.1 eV to 20 MeV luminosity (erg/s), assuming a subsequent decay law $\propto t^{-1.2}$). Conversion into line emission is much less efficient for high values of ξ , essentially because the emission saturates at a level determined by the recombination rate, which depends primarily just on n_p . For models 6, 7 the table gives the instantaneous specific line luminosities; the observed line-strengths would be reduced by a factor that allows for time-delay smearing in the integration over the large reprocessing shell. The luminosity in model 6 is typical of the afterglow luminosity after one day, so time-smearing leads to only a modest reduction in this case. On the other hand, the ultra-high luminosity in model 7 would be relevant only for the first 10 seconds; time-smearing would therefore reduce the observed line luminosity by a factor of up to $\sim 10^4$. In consequence, we would expect the prompt ultraluminous phase to make a negligible contribution to the Fe line emission from an extended shell. *Notes:* 1) np = no pairs; 2) nc = no comptonization; 3) ni = Nickel (Fe=0, Ni=20, see text). The line luminosity for model 6ni actually corresponds to the blend of nickel K lines.

efficiency of model 2nc is very nearly the same as that predicted by equation (2).

Question (1) can be addressed by comparing models 2 and 2nc. The effect of an accurate transfer treatment is to allow penetration of gamma rays due to the enhanced forward scattering probability of the KN cross section, and also to allow down-Comptonization of these penetrating photons at large column depths in the slab. For the estimates in the previous section we took $\tau_{Th} \simeq 1$ for the Thompson depth of the ionized part of the slab, but the Monte Carlo results show that photons penetrate to much greater depths. In Figure 2a we show a contour plot of photon intensity vs. energy and depth for model 2, which shows the incident radiation field is not depleted until $\tau_{Th} \simeq 10$. This accounts for the greater line intensity in model 2 than in model 2nc.

Figures 2a-d give more details of the spatial distributions of various physical quantities in model 2 for normal incidence. Figure 2a shows a contour plot of the ratio of photon mean intensity in the interior of the model to that at the surface as a function of energy and optical depth. The contour spacing is a factor of 1.6 in this figure, and dashed or solid contours indicate regions where the ratio is less than or greater than unity, respectively. This shows that photons below ~ 100 keV penetrate to $\tau_{Thompson} \sim 10$ for this choice of parameters before the intensity falls below 0.1 of the surface value. The mean intensity increases with increasing depth to a maximum at $\tau_{Thompson} \sim 3$. The flux would be zero in a pure scattering slab, but the effects of photoabsorption and reemission which shifts photons into the UV results in a non-zero net flux. Figure 2b shows the electron temperature vs. depth. Near the surface the gas approaches the Compton temperature, T_{IC} , which in this case is $\simeq 3 \times 10^8$ K. The blip near 10^5 K is a common feature in thermal equilibrium curves, being related to non-linearities in the heating and cooling from intermediate mass elements such as oxygen. Collisional cooling has a temperature dependence $\exp(-\text{const}/T)/\sqrt{T}$, and the local maxima in this function can lead to such bumps. Figure 2c shows the distribution of emissivity with depth in model 2. The various curves correspond to the components of the iron line from the hydrogen-like (dotted), helium-like (dot-dashed) and lower (dashed) ion stages. This reflects the dominance of recombination onto hydrogen-like iron in this model, owing to its large ionization parameter.

Figure 3 shows the total emitted spectrum ($\sim \varepsilon F_\varepsilon$) from model 2 for normal incidence. Clearly apparent are the He- and H-line iron lines, near 6.7 keV and 6.9 keV respectively, along with the L α analog line and recombination continuum from O VIII and lines from highly ionized Si and S. Interpretation of these results in terms of observations requires the introduction of additional assumptions. Although the most straightforward observational quantity that can be derived from the models is the total line flux emitted by the cloud, observations of the line are affected by Compton broadening of the line and

by the statistical significance of the line relative to the adjacent continuum. The line and continuum have differing dependence on reprocessing: the line must be reprocessed, while the continuum may include direct (unreprocessed) radiation. Moreover, we can envision various geometrical configurations for our model reprocessors even within the assumptions of a time-steady unbeamed continuum source. If the reprocessor has a covering fraction relative to the source less than unity, then the observed continuum near the line would likely be dominated by photons from the source. If the photons from the source are not directly observable, either due to time delays or due to beaming away from us, then the observed continuum near the line would be entirely due to Compton reflection and emission from the reprocessor. This simplified continuum scenario is what we consider in figures 3 and 4. Calculations of the line luminosity presented so far have illustrated the importance of Compton down-scattered gamma rays on the spectrum emitted in the cloud interior. Since this process occurs primarily at large depths in the reprocessor, line photons must traverse a corresponding column to escape, and scattering during this process broadens the line.

Figure 4a shows the spectrum in the vicinity of the iron line for model 2 at normal incidence and illustrates the effects of Comptonization of the line during escape. The solid curve shows the Comptonized profile, calculated self-consistently using a Monte-Carlo treatment of the photon escape from the cloud. Statistical uncertainties associated with the Monte Carlo treatment of scattering in this figure are negligibly small; we emit 10000 photons in each of the energy bins in our model; the few apparent gaps in the injected spectrum are due to slight mismatches in mapping between the energy grids used for the Monte Carlo and the xstar part of the calculation. For the purpose of treating the line escape from the cloud we have added the process of line resonant scattering to the Monte-Carlo calculation, so that we account for the enhancement to the photon path length and the probability of Compton scattering for resonance line photons such as Fe XXVI $\text{L}\alpha$. In doing so, we assume that each line scattering event is treated according to complete redistribution in the line Doppler core, and completely coherently in the line wings. In practice, the latter is unimportant, since Fe XXVI $\text{L}\alpha$ has maximum depth ~ 1000 , and the damping parameter is $\simeq 10^{-4}$. The results of the calculation of the unscattered luminosity of the Fe XXVI $\text{L}\alpha$ line, for all our models, is also given in the column of the Table labelled $L_{Fe}^{(ns)}$.

The results of Figure 4a for normal incidence show that the fraction of the line photons escaping unscattered is ~ 0.01 , and a comparable luminosity escapes as a broad comptonized continuum in the vicinity of the line. The narrow core of the 6.97 keV line has an equivalent width of $\simeq 0.2$ keV measured relative to the emergent flux averaged over the energy region shown in the figure, while the corresponding un-Comptonized line equivalent width is greater by a factor of ~ 30 . This figure, as well as Figure 2c, shows that although

various components of the line are emitted, the components at energies 6.7 keV (He-like) and below are more Comptonized than the components at 6.97 keV (H-like). This is due to the fact that the higher energy (H-like) component is emitted in the shallower, more highly ionized gas closer to the slab boundary, and therefore traverses a smaller depth as it escapes. The same effect applies to the continuum in the 5-8 keV energy range; these photons are predominantly emitted at large Thompson depths. The recombination continua are apparent in the injected spectrum but are smeared in the scattered spectrum. Resonance scattering does not affect the photons emitted in the higher Lyman series lines or the recombination continuum as much as the La line, so the ratio of these lines to the La analog line exceeds the recombination value in our simulations.

Our results differ from the calculations of McLaughlin et al. (2001) who considered Comptonization in a funnel geometry in that the reprocessors considered here have a Compton temperature $\simeq 10^8 \text{ K}$, so that the mean energy shift per scattering is large. Thus we do not predict easily identifiable spectral features associated with once- or twice-scattered photons, even for photons emitted at small depths. We have not explored different assumptions about the incident continuum shape, which could lead to reduced Compton temperature. We note, however, that it is unlikely that the temperature in the line emitting region will be low enough (i.e. $\leq 10^6 \text{ K}$) that the effects of thermal broadening in the Compton escape will be negligible.

We have also investigated the effects of reducing the line resonance scattering optical depth scale as might occur if, for example, the cloud had a large internal velocity dispersion $\sim 3000 \text{ km s}^{-1}$. We find that this affects the unscattered line luminosity by a factor ≤ 2 , reflecting the fact that the regions of large line depth are also regions of large continuum Thompson depth, and photons emitted in these regions are likely to be Comptonized even if they escape in a single flight. Although we consider these results to be an accurate prediction of the spectra corresponding to our assumed choice of parameters, they are likely to be quite sensitive to our assumptions regarding the reprocessor geometry, and these assumptions will produce the lowest fraction of escaping unscattered line photons. That is, we have assumed reprocessing in a plane parallel slab which is illuminated by normally incident continuum (but see below), for which the minimum Thompson depth for escape is always equal to the Thompson depth traversed by the incoming photons. The escaping unscattered fraction is very sensitive to this assumption. Other geometries, such as non-normal illumination, will produce a greater fraction of photons created at large depths which will escape unscattered. Therefore, we consider it likely that real reprocessors will produce lines with luminosities in a range between the unscattered luminosities and the total emitted luminosities (for normal incidence) given in the table.

Figure 4b gives an illustration of non-normal incidence effects, showing that when model 2 is recalculated using an incidence angle of 70° the luminosity of the iron line escaping unscattered increases by a factor ≥ 10 . Also notable in this figure is the fact that fraction of the unscattered He-like line, near 6.7 keV, is greater than for the H-like line at 6.97 keV. This is significantly different from the results for normal incidence, shown in figure 4a, for which the unscattered fraction of the He-like line is negligible. This is due to the differing scattering behaviors of the two lines: the H-like line is subject to resonance scattering while the forbidden and intercombination components of the He-like line are not, but the H-like line is emitted closer to the illuminated surface. At normal incidence the disparity in depths of emission is more important than the difference between resonance and non-resonance scattering, while at 70° the converse is true.

In the ninth column of the table we present the unscattered line luminosities calculated for a 70° incidence angle for each of the models. These show similar behavior to model 2: at 70° incidence the escaping unscattered flux is a factor $\sim 2\text{--}10$ less than the total emitted energy.

Our results shown in figure 4b are similar to those calculated by Ballantyne and Ramirez-Ruiz (2001) in the effects of Comptonization on the lines from H-like and He-like Fe. However, the difference between figures 4a and 4b illustrate the dependence of this result on the assumed geometry; at normal incidence the behavior is qualitatively different. Our models differ from those of Ballantyne and Ramirez-Ruiz (2001) in the choice of high energy cutoff for the illuminating continuum, and therefore in the Compton temperature. Our model continua extend to 10 MeV and have a Compton temperature $\simeq 3 \times 10^8$ K. A consequence of this is a lower recombination rate coefficient, and correspondingly lower reprocessing efficiency.

4.1. Pair Production

Pair production occurs due to γ, γ collisions between incident and reflected photons. We use rate coefficients taken from Coppi and Blandford (1990), equation (4.6):

$$R_{prod} \simeq c\sigma_{Th}(F/(c\varepsilon_{ave}))^2 f_1 f_2 \quad (6)$$

where ε_{ave} is the average photon energy, and f_1 and f_2 are factors less than unity describing the penetration of gamma rays and the albedo for upward photons, respectively. The rate of destruction by annihilation is approximately

$$R_{dest} \simeq \frac{3}{8} c \sigma_{Th} n_e n_p \quad (6)$$

Equating these gives an equilibrium pair density relative to protons of

$$n_e/n \simeq \frac{\xi}{c \varepsilon_{ave}} \sqrt{8f_1 f_2 / 3} \quad (7)$$

which is $n_e/n \simeq 10^5 \sqrt{8f_1 f_2 / 3}$ for $\xi = 10^4$, being proportional to ξ . Thus pair production can significantly enhance the total electron number density if the incident spectrum has a significant flux above ~ 1 MeV, and if the reprocessor albedo is not negligible. The effect of pairs on the iron line will be twofold: to enhance the iron recombination rate and thereby the line luminosity, and to decrease the mean free path of photons to Compton scattering. The Thompson depth in a pair-dominated cloud is proportional to $n_e R \propto \xi n R \propto L/R$, the compactness parameter (e.g. Coppi and Blandford 1990)

In order to evaluate quantitatively the effects of pairs we have included a calculation of the pair formation rate and of the equilibrium pair density self-consistently in all our models, using the following procedure: In our iterative procedure we initially set the continuum opacity and upward flux of gammas to be zero. As part of the Monte Carlo transfer calculation we calculate the number of pairs produced as a function of depth $N_{pairs}(z)$, and the number of upward photons vs. depth and energy, $N_{up}(\varepsilon, z)$. Pair production is calculated using the rate coefficient $R(x)$ from Coppi and Blandford equation 4.6 together with the number of upward photons vs. depth. The cross section for pair production is given by: $\sigma_{pair\ prod} = \max(R(x)F^{(n)}(\varepsilon, z))/c$, and the maximum is taken over all upward photon energies, and $F^{(n)}(\varepsilon, z)$ is the local upward photon number flux as a function of energy ε . The value of $F^{(n)}(\varepsilon, z)$ is calculated from the number of upward photons $N_{up}(\varepsilon, z)$ by $F^{(n)}(\varepsilon, z) = F_{inc}^{(n)} N_{up}(\varepsilon, z) / N_{tot}$. This step is repeated a number of times (~ 10) to self-consistently calculate the pairproduction and upward flux of gammas. Pair production is included in the xstar calculation by converting the number of pairs created at each depth to a rate by $R_{pair\ prod}(z) = F_{inc}^{(n)} N_{pairs}(z) / N_{tot}$. Destruction (annihilation) is calculated using the rate given in Coppi and Blandford (3.7). The equilibrium pair density is added to the ordinary free electron density and allowed to contribute to recombination, line formation, etc. This is equivalent to assuming that the pairs thermalize before annihilating. This can be justified by noting that the timescale for slowing down a fast (~ 1 MeV) particle in a fully ionized gas is approximately $10^3 n_{12}^{-1}$ s, while the e^+e^- annihilation timescale is longer by a factor \sim a few (Bussard et al., 1979). Both Monte-Carlo and photoionization steps are repeated a number of times (~ 4) to self-consistently calculate transfer, ionization , pair production/annihilation, etc. We also implement a self-consistent updating of the optical

depth scale when iterating between the xstar and Monte-Carlo parts of the problem. This is done by performing the Monte-Carlo in optical depth space, so the only density dependent quantity is the ratio of pair cross section to scattering cross section for each flight. The pair production rate is found to converge to within $\simeq 10\%$ after 3 iterations between the Compton and xstar parts of the calculation if the reflected flux is initially assumed to be zero.

The effects of pairs are shown in the table by comparing models 2, 5 and 7 with the corresponding models which are identical but which have the effects of pairs turned off (models 2np, 5np and 7np respectively). At each point in the model the local effect of pairs is to increase the recombination rate and thereby to decrease the level of ionization of the gas, increasing the density of ions such as Fe XXVI and Fe XXV. Since the photoionization heating rate increases proportional to these abundances, the effect is to increase the gas temperature. This, in turn, increases the optical depth to photoabsorption by highly ionized iron, thereby reducing the photoionization heating rate deeper in the cloud. Pairs cause the temperature to be greater at small depth, and lower at large depth than would otherwise be the case. Since the iron line emissivity is generally a decreasing function of temperature for photoionized models, the two regions will have competing effects on the total line luminosity. The results of the Table show that the line luminosity is unchanged by pairs for models 2 and 7, and is slightly decreased by pairs for model 5. This difference between models can be attributed to the greater compactness of model 5 compared with either model 2 or 7. The unscattered iron line luminosity is affected more by the neglect of pairs than is the emitted line luminosity, reflecting the fact that pairs affect the optical depth scale more than the temperature distribution. An additional effect of pairs, for reprocessors with densities less than we consider here, is to reduce the Compton mean free path relative to the cloud size. This can allow clouds with low (proton) column densities to be Thompson thick.

5. Effects of Continuum Variability and Time Delays

Most of the results discussed so far are independent of whether the observer sees the radiation from the entire reprocessor at the same time, assuming an illuminating radiation which is constant in time. In reality, the illuminating radiation flux level changes in time, typically being a smoothly decreasing function of time. For the “nearby reprocessor” models 1-5, the finite light-travel time differences between different parts of the reprocessor are negligible for observer times $t_{obs} \gtrsim 10^2 - 10^3$ s, particularly if the radiation arises from a limited range of solid angles, such as a funnel. However, for

the “distant reprocessor” models 6-7, the finite light-travel time between the continuum source and the shell means that the observer sees simultaneously different parts of the reprocessor which are illuminated by the continuum at different source times. The regions nearest to the observers are illuminated by a continuum corresponding to later source times than the regions farther from the observer. This convolution can be described by an equation of the form $L(t) = \frac{f}{2} \int_{\theta_{min}}^1 \sin \theta \, d\theta \int_0^t dt' L_{line}(\theta, t') \delta(t - t' - R(1 - \cos \theta)/c) = \frac{f}{2} \frac{c}{R} \int_{\max(1, t-2R/c)}^t dt' L_{line}(\cos^{-1}(1 - \frac{c}{R}(t - t')), t')$, where $L_{line}(\theta, t)$ is the emitted luminosity from the surface of the reprocessor as a function of observing angle and time, f is a factor ≤ 1 which takes into account the fact that the reprocessor can be clumpy, and as seen by the source it can cover less than 4π , and the line emission is not isotropic. The integral is over the surface of the reprocessing shell illuminated by the continuum, which may be beamed (e.g. Weth, *et al.* 2000). The effect of time delays have been considered also by Lazzati *et al.* (1999), Böttcher (2000), and in a torus geometry by Böttcher & Fryer (2001). The main effect of the time delays is that the peak line (or reprocessed continuum) luminosity is smaller than the line fluxes given in Table 1, due to smearing by a factor of the order $t_0/t_{peak} \sim 10^{-1} - 10^{-4}$, where t_0 is the duration of the initial burst and $t_{peak} \sim (2R/c)(1 - \sin \theta_j) \sim$ day, depending on the model. Thus, in such models we expect that the observed $L_{Fe} \lesssim 10^{43}$ erg/s. A quantitative discussion of the Fe light curves is affected by uncertainties in the model details. However, detailed calculations of specific models (Weth *et al.* 2000, Böttcher 2000, Böttcher & Fryer 2001, etc) confirm the above approximate estimate of $L_{Fe} \lesssim 10^{43}$ erg/s if solar abundances are used in a “distant reprocessor” scenario.

6. Abundance Effects

The Fe line luminosities calculated here are based on solar abundances, and would be boosted by the appropriate factor if supersolar values are taken. In the nearby reprocessor models 1-5 this is not necessary, as the line intensities are in the observed range even with the solar abundances used. However, in the distant reprocessor models 6-7 (see Table 1) after applying a $10^{-2} - 10^{-3}$ dilution factor due to the time delay smearing discussed in the previous section, a factor 10-100 increase relative to solar Fe abundance would be required to meet the observed line luminosities. (Even so, a total shell mass of $\sim 1 - 10 M_\odot$ is implied, so that a simple increase in the density while retaining solar abundances would appear less plausible in this scenario than an increase in the Fe abundance).

Another effect, of relevance in the distant reprocessor scenarios, if associated with recent supernova events (e.g. Piro *et al.* 2000, Vietri *et al.* 2000) is the production of large

amounts of iron via the decay of nickel and cobalt, after a longer delay of order 50 days. Although our models so far all have solar abundances of iron and neglect nickel and cobalt, we can crudely test for such abundance effects by modifying the abundances in the model scenario which most nearly resembles the supernova reprocessor. We have done this in model 6ni in which we have used the conditions for model 6 but we have set the iron abundance to 0 and instead chosen a nickel abundance such that the number density of nickel ions is the same as the number density of iron ions in model 6. This corresponds to a 20 times overabundance of nickel relative to the solar values of Grevesse et al (1996). (Owing to uncertainties in atomic data, xstar does not include cobalt, and so we cannot directly test scenarios involving mixtures of this element). The results are given in Table 1, in which the line strengths in the last column for model 6ni correspond to nickel rather than iron. We find that the dominant nickel line is the helium-like complex at 7.78 keV, and the strength of this feature slightly exceeds the strength of the Fe XXVI line in model 6. This feature appears prominently in the model spectrum, and would lead to a greater inferred redshift for the source if it were the true origin of the feature observed in eg. GRB991216.

7. Discussion

The results shown in the previous sections demonstrate that iron line luminosities of $\sim 10^{43} - 10^{45}$ erg s $^{-1}$, comparable to the luminosities observed so far (eg. Piro et al. 2000), can be produced by dense reprocessing gas in the vicinity of gamma ray burst sources. The exact shape of the line, and the fraction escaping in a narrow core, are sensitive to the details of the geometry of the reprocessor. This lends plausibility to the assumed model density and ionization parameters in “nearby reprocessor” scenarios such as the jet plus bubble model (Mészáros and Rees, 2001) and the delayed jet model (Rees and Mészáros , 2000), which as shown here, are able to produce the required Fe line luminosities using solar chemical abundances or enrichment factors which are in the range 1-10. In the “distant reprocessor” scenarios involving, e.g. a supernova or wind related shell (Vietri et al 2001, Piro et al, 2000, Weth et al, 2000, Böttcher, 2000, Böttcher and Fryer 2001) our results in Table 1 obtained with solar abundances indicate that, accounting for time-delay dilution, at least a 10-100 times Fe overabundance over solar values would be required to explain the observed Fe line luminosities.

Further diagnostic information about the reprocessor is available from detections or limits on absorption features due to bound-bound or bound-free transitions of iron. For the physical conditions envisaged in this paper, photoionization equilibrium is a good approximation, and non-equilibrium effects are expected to be small. With different model

assumptions, however, these might play a role, e.g. possibly in enhancing the radiation recombination (free-bound) edge (Yonetoku, *et al.*, 2001), Yoshida *et al.*, 2001), or in producing an absorbing column which varies with time after the initial burst onset (Lazzati and Perna 2001). Enhanced recombination may occur if the electron temperature is (very) low compared with the ionization temperature, which is less likely under photoionization conditions, but may be possible if the gas undergoes sudden rarefaction and adiabatic cooling of the electrons. The data on GRB 991216 which they discuss is close to what is predicted by the simple photoionization equilibrium models discussed here. In general, the bound-free absorption cross section from the K shell of iron is not a sensitive function of the ionization state of iron, and it is comparable with the Thompson cross section if the abundances are cosmic and if the ionization is favorable. Since all the reprocessors described in the previous section are effectively semi-infinite, they will not transmit efficiently near iron and so absorption features (e.g. as reported, at the 3σ level, by Amati *et al.*, 2000) are not expected from these simplified models. Absorption features would be imprinted on the reflected continuum from thick reprocessors at ionization parameters lower than those we examine here, e.g. $\log(\xi) \leq 100$, but this does not appear to be compatible with conditions inferred from observed emission lines. However, if the Thompson depth of the reprocessor were, at least temporarily, close to unity (as might be expected in a nearby reprocessor model, as the jet and the prompt portion of its relativistic waste bubble breaks through the last few optical depths at increasing angles), such features may also be naturally expected.

We are grateful to Xin-min Hua for use of the Comptonization code, D. Ballantyne and E. Ramirez-Ruiz for discussions, and to NASA NAG5-9192 and the Royal Society for support.

REFERENCES

Amati, L, *et al.*, 2000, *Science*, 290, 953.

Ballantyne, D., and Ramirez-Ruiz, 2001 *Ap.J. Lett.* 559, 83

Ballantyne, D., Ross, R., and Fabian, A., 2001 *MNRAS* 327, 10.

Bautista, M., & Kallman, T. 2001, *ApJ* 134, 139

Böttcher, M , 2000, *ApJ* 539, 102

Böttcher, M and Fryer, C, 2001, *ApJ* 547, 338

Bussard, R., Ramaty, R., and Drachman, R., 1979 *ApJ* 228 928

Coppi, P., and Blandford, R., 1990 *MNRAS* 245 453

Grevesse, N., Noels, A., and Sauval, A., 1996, in “Cosmic Abundances” ASP Conference Series, 99, S. Holt and G. Sonneborn, eds.

Guilbert, P., 1986 *MNRAS* 218 171

Hua, X., 1997 *Comp Phys* 11, 660

Kallman, T., and Bautista, M., 2001, *ApJ* 133, 221

Kallman, T., and McCray, R., 1982, *Ap. J. Supp.*, 50, 49

Lazzati, D. *et al.*(1999) *MNRAS*, 304, L31

Lazzati, D. and Perna, R. (2001) preprint.

McLaughlin, G.C., et al., 2001, *Ap. J.* submitted

Mészáros , P., and Rees, M., 2001, *ApJ(Letters)*, 556, L37

Nayakshin, S., et al., 2000 *ApJ* 537 833

Piro, L., et al, 1999, *Ap J (Letters)*, 514, L73

Piro, L., et al, 2000 *Science* 290 955

Rees, M.J. and Mészáros , P, 2000, *ApJ (Letters)*, 545, L73

Tarter, C. B., Tucker, W, & Salpeter, E. 1969, *ApJ*, 156, 943

Vietri, M., *et al.*, 2001 *ApJ (Letters)*, 550 L43

Weth, C., *et al.*, 2000, *ApJ* 534, 581

Yonetoku, D, *et al.*, 2001, *ApJ*, 557, L23

Yoshida, A, *et al.*, 1999, *Astron. Ap.*, 138, 433

Yoshida, A, *et al.*, 2001, *ApJ*, 557, L27

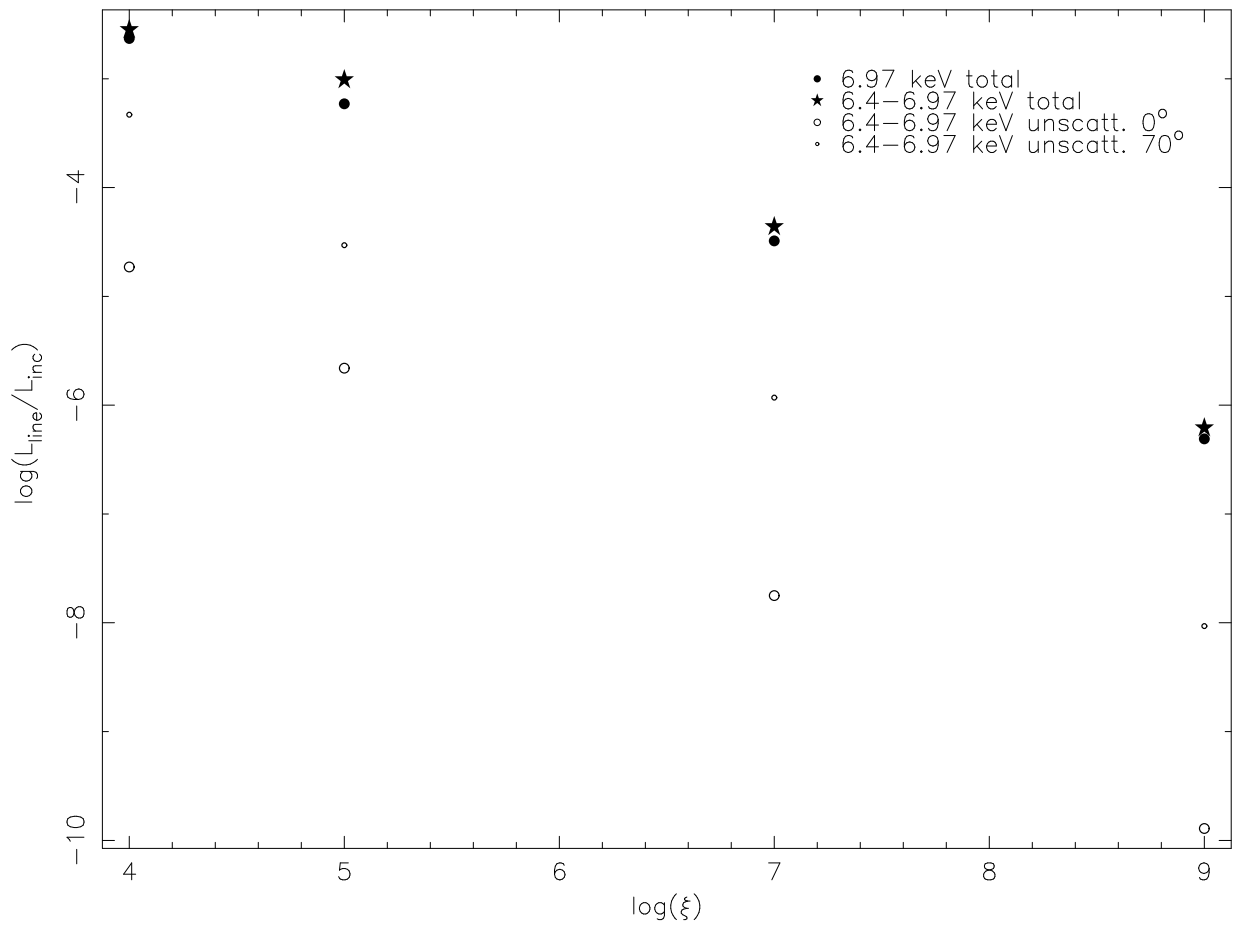


Fig. 1.— Line reprocessing efficiency vs. ionization parameter for the nearby models shown in the table.

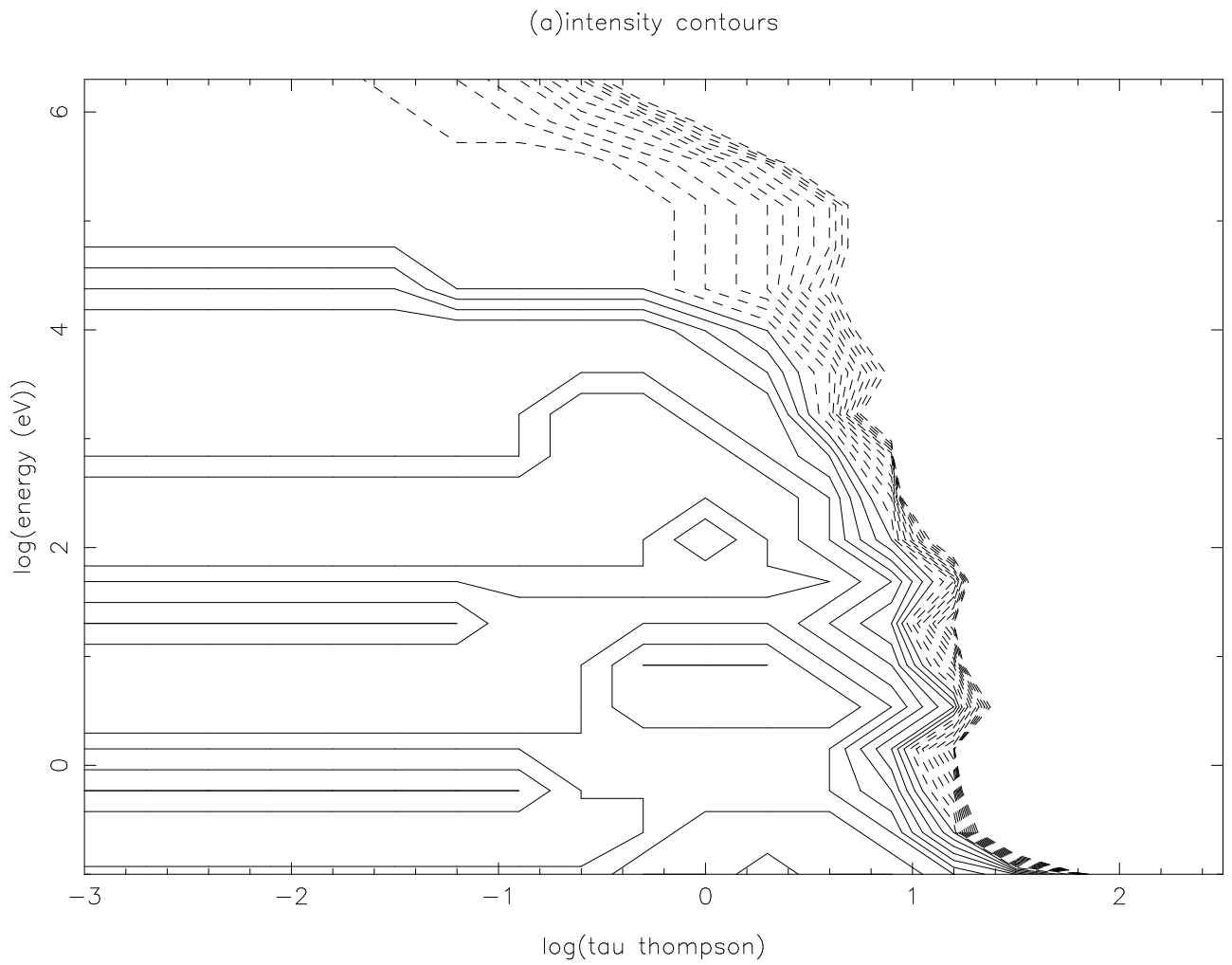


Fig. 2.— (a) Contours of constant mean intensity relative to the incident intensity vs. energy and Thomson optical depth for model 2. Contours interval is 0.2 dex. Solid contours correspond to mean intensity greater than incident and demonstrate the effects of Compton downscattering. Dashed contours correspond to mean intensity less than incident and demonstrate the effects of attenuation and Compton reflection.

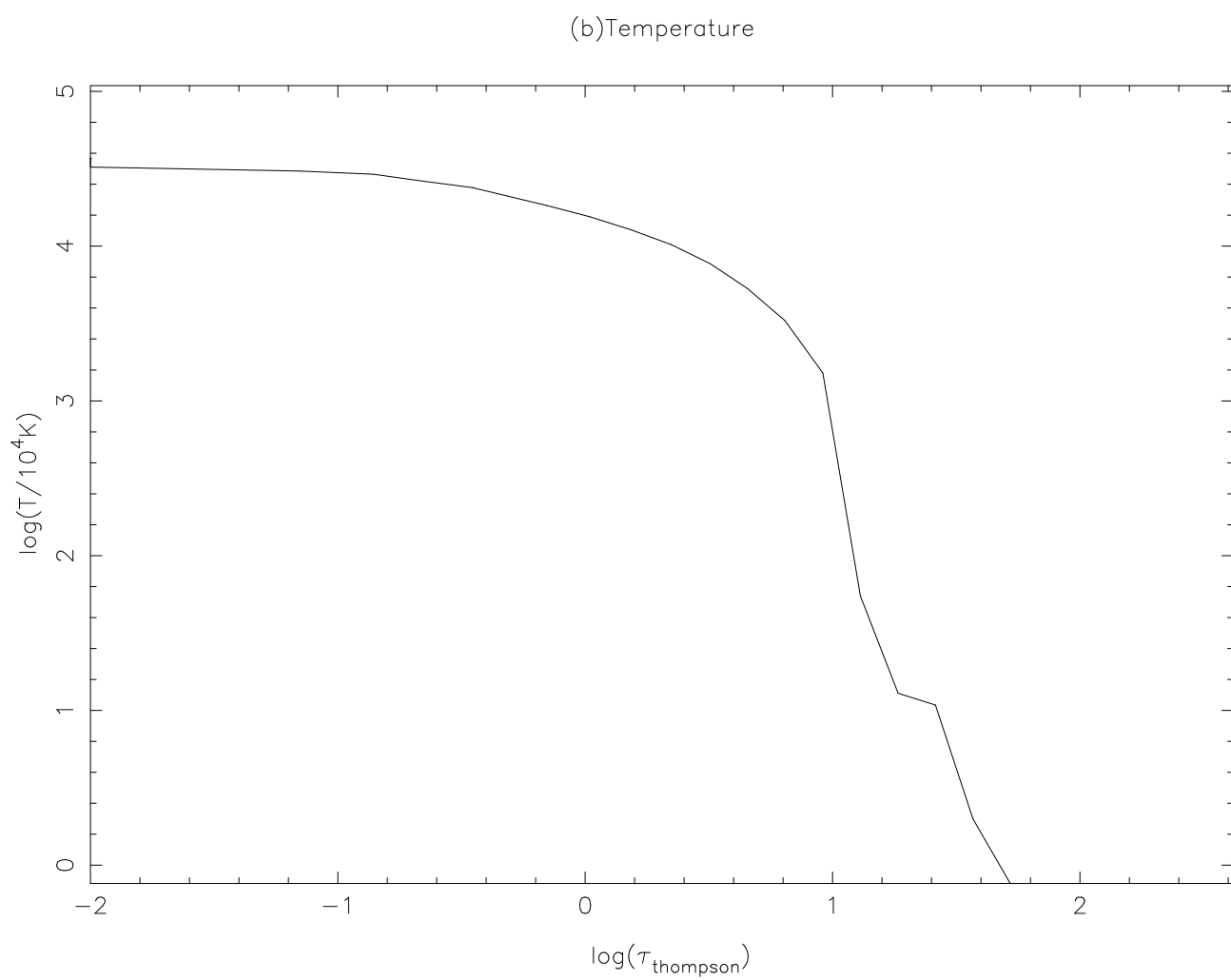


Fig. 2.— (b) Temperature vs. depth for model 2.

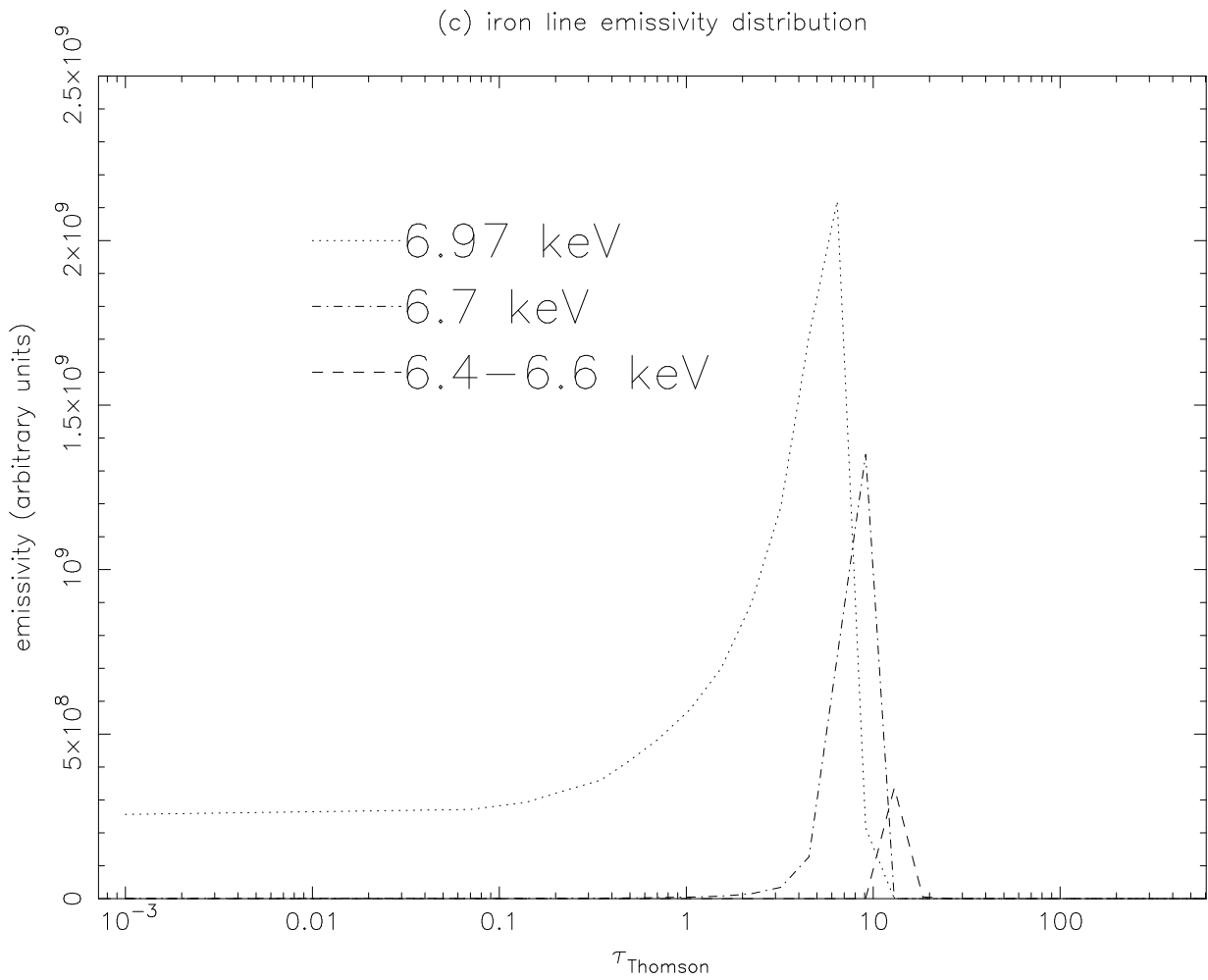


Fig. 2.— (c) Iron line emissivity vs. depth for model 2 for the various components: 6.97 keV (hydrogen-like iron), 6.7 keV (He-like iron), and 6.4 – 6.6 keV (all lower stages).

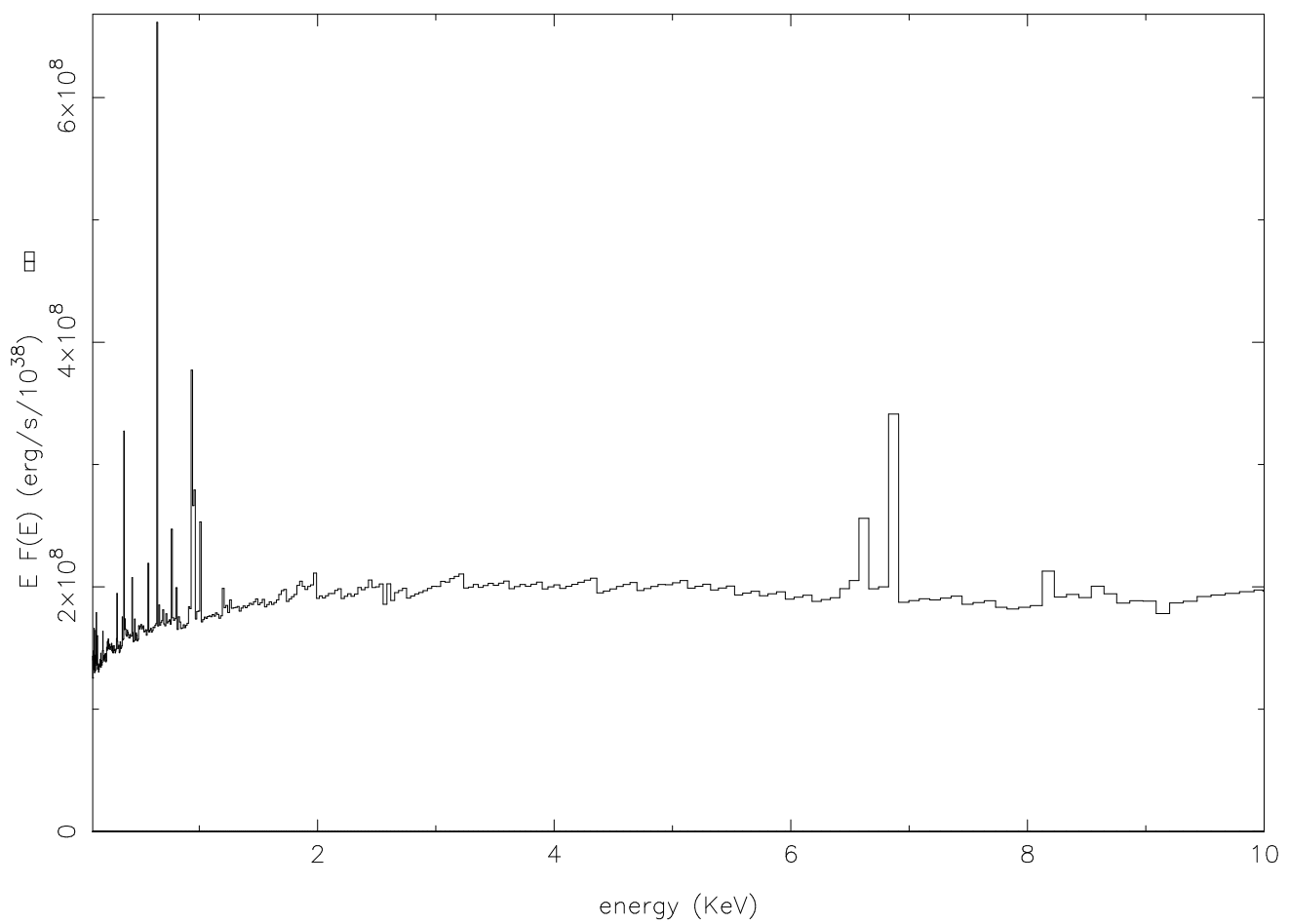


Fig. 3.— Reflected spectrum from model 2 for normal incidence.

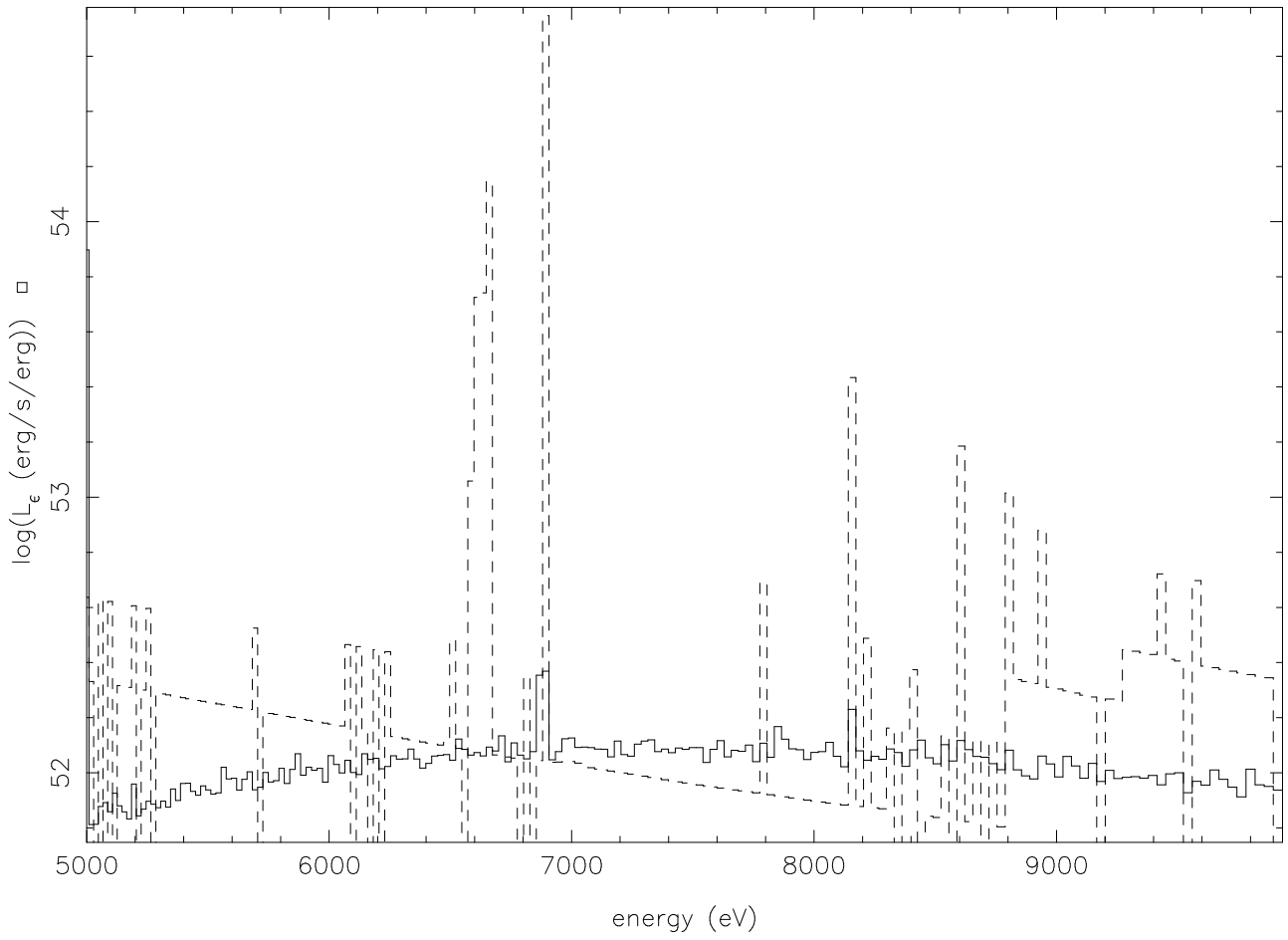


Fig. 4.— a) Reflected spectrum from model 2 (normal incidence) in the energy region near the iron line, showing the effects of Comptonization of the escaping photons (solid curve) and the total emitted spectrum (dashed curve).

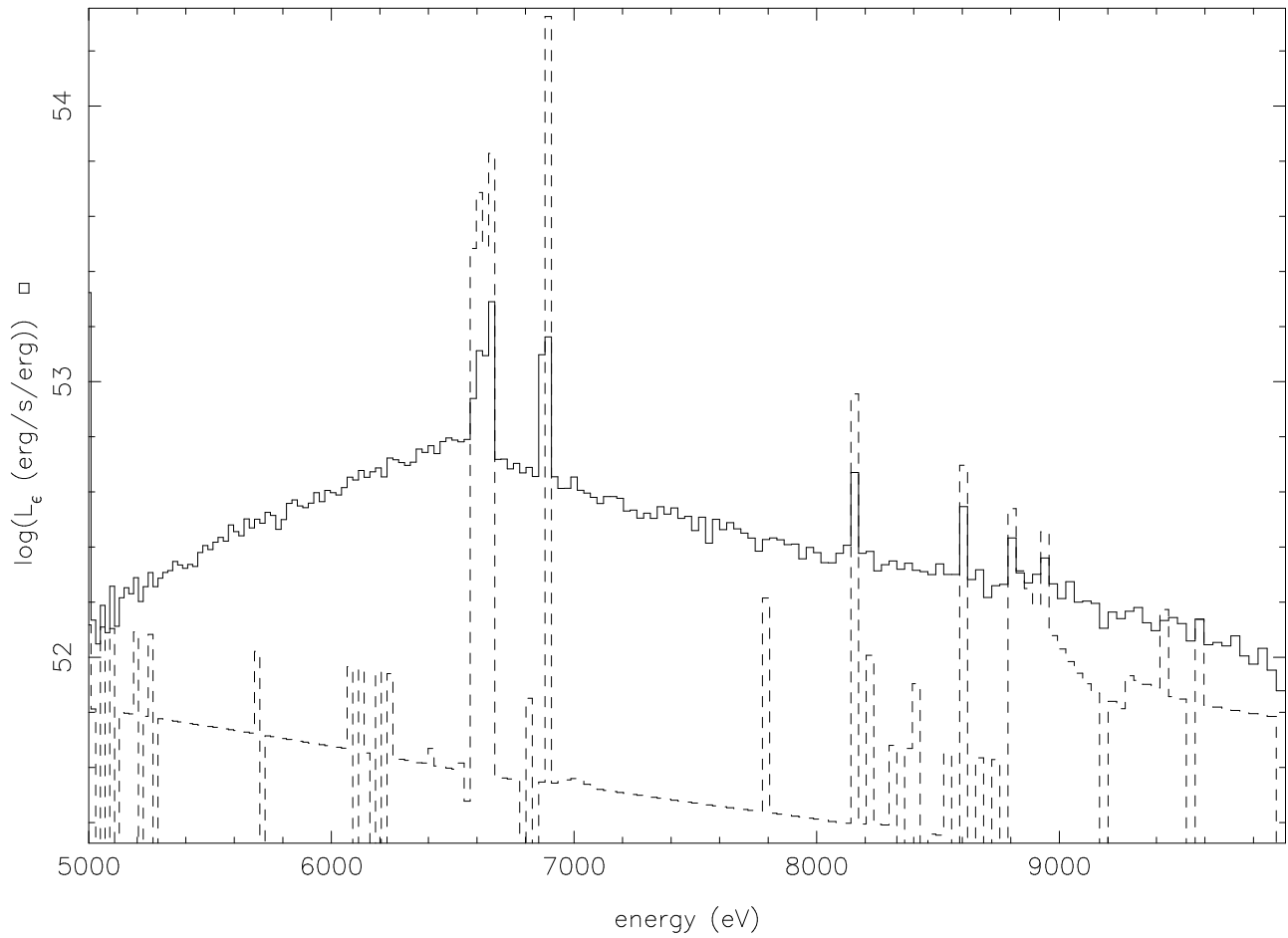


Fig. 4.— b) Reflected spectrum from model 2 for a 70 degree incidence angle, showing the energy region near the iron line. In this case all depths affecting escape of photons are correspondingly reduced by a factor of 5. The Comptonized escaping spectrum is shown as the solid curve and the total emitted spectrum is the dashed curve.